



OPEN

Entropy generation and flow characteristics of Powell Eyring fluid under effects of time scale and viscosities parameters

Mohsan Hassan¹, Muhammad Ahsan¹, Usman^{2✉}, Metib Alghamdi³ & Taseer Muhammad³

Shear thinning fluids are widely used in the food and polymer industries due to their unique flow characteristics. The flow behavior of these fluids has been commonly studied using the Powell Eyring model under a small shear rate assumption. However, this assumption is not always valid. In this study, we explore the transport characteristics of a Powell Eyring fluid over a variable thicker sheet, not only at small shear rates but also at medium and high shear rates. Furthermore, we calculate the rate of entropy generation based on the assumptions. Generalized Powell–Eyring model of viscosity is used for the fluid, representing the re-arrangements of molecules in the forward and backward directions through the theory of potential energy. The model concludes the sensitivity of the viscosity from zero to infinite shear rate along time scale and exponent parameters. The model is used in the transport phenomena equations. The solution of the equation is obtained by using the numerical method and used to calculate the rate of entropy generation. The results are presented in the form of velocity and temperature profiles, the average rate of entropy generation, skin friction coefficient and Nusselt number under the influence of various viscosity parameters. It is found that velocity and temperature profiles are decreased and increased respectively against the time scale parameter.

Fluid flow is a fundamental phenomenon in the chemical process industry, where the flow pattern and the type of liquid/fluid significantly impact the equipment layout, process performance, and economic situation. To efficiently and safely run a chemical plant, it is crucial to anticipate the behavior of fluid flow, along with prior knowledge of heat and mass transfer and boundary conditions. While predicting the behavior of Newtonian liquids, such as water, alcohols, and esters, is relatively straightforward, it becomes much more challenging for non-Newtonian fluids with complex rheological patterns and flow behaviors^{1,2}. Shear thinning is a common phenomenon observed in non-Newtonian fluids, wherein the viscosity of the fluid decreases with an increase in shear rate. The viscosity of shear-thinning fluids is a function of shear rate and exhibits Newtonian behavior at very low and high shear rate values. Shear thinning fluids have numerous examples and applications in daily life and the food industry, such as melted chocolate, tomato paste in the ketchup industry, and yoghurt. Polymer melts of high- and low-density polyethylene, nylon, polyester, and polystyrene are a few examples of shear-thinning fluids. Other examples of shear-thinning liquids in the cosmetic industry include nail polish, toothpaste, and moisturizing lotions. Given the significant applications of shear-thinning fluids, it is essential to investigate their rheological and flow behaviors and patterns to ensure smooth operation in the chemical process industry. Accurately predicting and understanding the behavior of these fluids can lead to simpler equipment design, avoiding unnecessary complexity throughout the process and ensuring optimal process performance and safety.

There exist numerous mathematical models in the literature to describe the rheological behavior of shear-thinning fluids. The first model proposed by Ostwald in 1929 established a simple relation between shear stress and shear rate³. This model, commonly known as the “power law”, became the basis for various viscometers and rheometers used to gather rheological data for different shear-thinning fluids. However, the power law is not suitable for predicting the behavior of shear-thinning fluids at low and high shear rate values. In 1965, Cross proposed another mathematical expression to describe the rheological behavior of inelastic fluids, which is comparatively better than the power law in terms of predicting the rheological properties of shear-thinning

¹Department of Mathematics, COMSATS University Islamabad, Lahore Campus, Lahore 54000, Pakistan. ²Department of Computer Science, National University of Sciences and Technology, Balochistan Campus (NBC), Quetta 87300, Pakistan. ³Department of Mathematics, College of Sciences, King Khalid University, Abha 61413, Saudi Arabia. ✉email: usman.malik.ms@gmail.com

fluids at low and high shear rate values⁴. Carreau introduced a model in 1972 based on the molecular structure of shear-thinning fluids⁵. By considering the molecular structure, it is possible to predict the rheological behavior of these fluids by establishing a relationship between viscosity and shear rate. Another general relation between viscosity and shear rate, in the form of an inverse hyperbolic sine, is presented in references^{6,7} and defined as

$$\mu = \mu_\infty + (\mu_0 - \mu_\infty) \left(\frac{\sinh^{-1}(\lambda|\bar{\gamma}|)}{\lambda|\bar{\gamma}|} \right)^\sigma \tag{1}$$

where μ_0 and μ_∞ are viscosities at low and high shear rate respectively, $\bar{\gamma}$ is shear rate, λ is time scale parameter and σ is exponent parameter. The Sutterby model is attained when $\mu_\infty = 0$ and The Eyring model is gotten when $\mu_\infty = 0$ and $\sigma = 1$. The Eyring–Powell model is represented in Eq. (1) when $\sigma = 1$. Equation (1) is extensively used to predict the flow patterns of shear thinning non-Newtonian fluids for different applications as follows in Table 1.

The studies mentioned above indicate that Eq. (1) has been extensively examined in fluid flow problems across various geometries, subject to certain assumptions $\sigma = 1, \mu_\infty = 0$ and $\lambda|\bar{\gamma}| \ll 1$. The viscosity of some shear-thinning liquids can be altered by a factor of three to four relative to the shear rate, making it impossible to disregard such a substantial change in viscosity during the processing of polymer melts or lubes. Consequently, the aforementioned assumptions cannot be considered universally applicable. The present problem’s objective is to investigate Eyring–Powell fluid flow with heat transfer while taking into account viscosity at low shear rates, which has not been previously addressed. The flow is analyzed over a variable nonlinear thicker stretching sheet, with boundary layer assumptions applied due to the proximity of the flow to the wall. The problem consists of highly nonlinear differential equations that are solved using numerical techniques. The results are expressed as velocity and temperature equations, which are then used to calculate physical quantities.

Mathematical model

Consider the incompressible, steady-state and laminar boundary layer flow of the non-Newtonian fluid through the Generalized Powell–Eyring model over a variable thicker sheet. The flow geometry is shown in Fig. 1.

The sheet is subjected to stretching at a variable velocity, denoted by a function $u_w = a(\bar{x} + b)^m$. Additionally, the thickness of the sheet varies with a specific function $y = A(\bar{x} + b)^{\frac{1-m}{2}}$. It is assumed that the temperature of the sheet remains constant T_w , and is greater than the temperature of the inviscid region denoted by T_∞ .

The mathematical flow model is based on partial differential equations that represent continuity, momentum, and energy equations as follows

$$\bar{u}_x + \bar{v}_y = 0, \tag{2}$$

$$\rho(\bar{u}\bar{u}_x + \bar{v}\bar{u}_y) = -\bar{p}_x + (\bar{\tau}_{11})_x + (\bar{\tau}_{12})_y, \tag{3}$$

$$\rho(\bar{u}\bar{v}_x + \bar{v}\bar{v}_y) = -\bar{p}_y + (\bar{\tau}_{21})_x + (\bar{\tau}_{22})_y, \tag{4}$$

$$\rho C_p(\bar{u}\bar{T}_x + \bar{v}\bar{T}_y) = k(\bar{T}_{xx} + \bar{T}_{yy}) + \bar{\phi}. \tag{5}$$

Authors	Model	Geometry	Remarks/investigations
Arshad et al. ⁸	$\sigma = 1, \mu_\infty = 0, \lambda \bar{\gamma} \ll 1, \sinh^{-1}(\lambda \bar{\gamma}) \approx \lambda \bar{\gamma} - \frac{1}{6}(\lambda \bar{\gamma})^3$	Peristaltic parallel walls	Thermal behavior of hybrid nanomaterial in fluid flow
Mubbashar Nazeer et al. ⁹	$\sigma = 1, \mu_\infty = 0, \lambda \bar{\gamma} \ll 1, \sinh^{-1}(\lambda \bar{\gamma}) \approx \lambda \bar{\gamma} - \frac{1}{6}(\lambda \bar{\gamma})^3$	Parallel walls	Comparative study of Crossflow of heat and mass
Oke et al. ¹⁰	$\sigma > 1, \mu_\infty = 0, \lambda \bar{\gamma} \ll 1, \sinh^{-1}(\lambda \bar{\gamma}) \approx \lambda \bar{\gamma} - \frac{1}{6}(\lambda \bar{\gamma})^3$	Linear stretching sheet	Shear thinning and thickening effects of heat and mass flow
Rahimi et al. ¹¹	$\sigma = 1, \mu_\infty = 0, \lambda \bar{\gamma} \ll 1, \sinh^{-1}(\lambda \bar{\gamma}) \approx \lambda \bar{\gamma} - \frac{1}{6}(\lambda \bar{\gamma})^3$	Linear stretching sheet	Solution by collocation method of boundary layer fluid flow
Verma et al. ¹²	$\sigma = 1, \mu_\infty = 0, \lambda \bar{\gamma} \ll 1, \sinh^{-1}(\lambda \bar{\gamma}) \approx \lambda \bar{\gamma} - \frac{1}{6}(\lambda \bar{\gamma})^3$	Moving plate	Stability analysis and multiple solutions of nanofluid flow
Ali Akgul ¹³	$\sigma = 1, \mu_\infty = 0, \lambda \bar{\gamma} \ll 1, \sinh^{-1}(\lambda \bar{\gamma}) \approx \lambda \bar{\gamma} - \frac{1}{6}(\lambda \bar{\gamma})^3$	Linear stretching sheet	Solution of boundary layer flow by Hilbert space method
Imran et al. ¹⁴	$\sigma = 1, \mu_\infty = 0, \lambda \bar{\gamma} \ll 1, \sinh^{-1}(\lambda \bar{\gamma}) \approx \lambda \bar{\gamma} - \frac{1}{6}(\lambda \bar{\gamma})^3$	Oscillatory curved sheet	Heat transfer analysis through Fourier and Fick model
Ibrahim and Hindebu ¹⁵	$\sigma = 1, \mu_\infty = 0, \lambda \bar{\gamma} \ll 1, \sinh^{-1}(\lambda \bar{\gamma}) \approx \lambda \bar{\gamma} - \frac{1}{6}(\lambda \bar{\gamma})^3$	Stretching cylinder	Heat transfer analysis in nanofluid through the Cattaneo-Christov model
Kumar et al. ¹⁶	$\sigma = 1, \mu_\infty = 0, \lambda \bar{\gamma} \ll 1, \sinh^{-1}(\lambda \bar{\gamma}) \approx \lambda \bar{\gamma} - \frac{1}{6}(\lambda \bar{\gamma})^3$	Annulus	Magnetic and rotation effects on mass flow
Gholinia et al. ¹⁷	$\sigma = 1, \mu_\infty = 0, \lambda \bar{\gamma} \ll 1, \sinh^{-1}(\lambda \bar{\gamma}) \approx \lambda \bar{\gamma} - \frac{1}{6}(\lambda \bar{\gamma})^3$	Rotating disk	Homogeneous–heterogeneous reactions on heat and mass flow
Salawu et al. ¹⁸	$\sigma = 1, \mu_\infty = 0, \lambda \bar{\gamma} \ll 1, \sinh^{-1}(\lambda \bar{\gamma}) \approx \lambda \bar{\gamma} - \frac{1}{6}(\lambda \bar{\gamma})^3$	Channel	Entropy generation of fluid under magnetic effects
Madhu et al. ¹⁹	$\sigma = 1, \mu_\infty = 0, \lambda \bar{\gamma} \ll 1, \sinh^{-1}(\lambda \bar{\gamma}) \approx \lambda \bar{\gamma} - \frac{1}{6}(\lambda \bar{\gamma})^3$	Microchannel	Heat and mass transfer in the presence of a thermal heat source
Çolak et al. ²⁰	$\sigma = 1, \mu_\infty = 0, \lambda \bar{\gamma} \ll 1, \sinh^{-1}(\lambda \bar{\gamma}) \approx \lambda \bar{\gamma} - \frac{1}{6}(\lambda \bar{\gamma})^3$	Stretching sheet	Bioconvective in nanofluid

Table 1. The non-Newtonian Eyring–Powell model over diverse geometries^{8–20}.

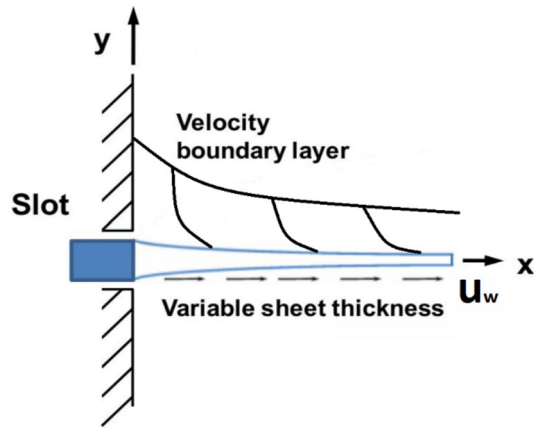


Figure 1. The flow geometry for the problem.

In the above, the shear stresses τ_{ij} for the Generalized Powell–Eyring model are defined as

$$\begin{aligned} \bar{\tau}_{11} &= \mu_\infty + (\mu_o - \mu_\infty) \left(\frac{\sinh^{-1}(\lambda|\bar{\gamma}|)}{\lambda|\bar{\gamma}|} \right)^\sigma (2\bar{u}_{\bar{x}}) \\ \bar{\tau}_{12} = \bar{\tau}_{21} &= \mu_\infty + (\mu_o - \mu_\infty) \left(\frac{\sinh^{-1}(\lambda|\bar{\gamma}|)}{\lambda|\bar{\gamma}|} \right)^\sigma (\bar{u}_{\bar{y}} + \bar{v}_{\bar{x}}) \\ \bar{\tau}_{22} &= \mu_\infty + (\mu_o - \mu_\infty) \left(\frac{\sinh^{-1}(\lambda|\bar{\gamma}|)}{\lambda|\bar{\gamma}|} \right)^\sigma (2\bar{v}_{\bar{y}}) \end{aligned} \tag{6}$$

and viscous dissipation $\bar{\phi}$ is written as

$$\bar{\phi} = \left\{ \mu_\infty + (\mu_o - \mu_\infty) \left(\frac{\sinh^{-1}(\lambda|\bar{\gamma}|)}{\lambda|\bar{\gamma}|} \right)^\sigma \right\} (2\bar{v}_{\bar{y}}^2 + (\bar{u}_{\bar{y}} + \bar{v}_{\bar{x}})^2 + 2\bar{u}_{\bar{x}}^2). \tag{7}$$

In view of Eqs. (5) and (6), Eqs. (2)–(4) are written as

$$\begin{aligned} \rho(\bar{u}\bar{u}_{\bar{x}} + \bar{v}\bar{u}_{\bar{y}}) &= -\bar{p}_{\bar{x}} + \left(\mu_\infty + (\mu_o - \mu_\infty) \left(\frac{\sinh^{-1}(\lambda|\bar{\gamma}|)}{\lambda|\bar{\gamma}|} \right)^\sigma (2\bar{u}_{\bar{x}}) \right)_{\bar{x}} \\ &\quad + \left(\mu_\infty + (\mu_o - \mu_\infty) \left(\frac{\sinh^{-1}(\lambda|\bar{\gamma}|)}{\lambda|\bar{\gamma}|} \right)^\sigma (\bar{u}_{\bar{y}} + \bar{v}_{\bar{x}}) \right)_{\bar{y}}, \end{aligned} \tag{8}$$

$$\begin{aligned} \rho(\bar{u}\bar{v}_{\bar{x}} + \bar{v}\bar{v}_{\bar{y}}) &= -\bar{p}_{\bar{y}} + \left(\mu_\infty + (\mu_o - \mu_\infty) \left(\frac{\sinh^{-1}(\lambda|\bar{\gamma}|)}{\lambda|\bar{\gamma}|} \right)^\sigma (\bar{u}_{\bar{y}} + \bar{v}_{\bar{x}}) \right)_{\bar{x}} \\ &\quad + \left(\mu_\infty + (\mu_o - \mu_\infty) \left(\frac{\sinh^{-1}(\lambda|\bar{\gamma}|)}{\lambda|\bar{\gamma}|} \right)^\sigma (2\bar{v}_{\bar{y}}) \right)_{\bar{y}}, \end{aligned} \tag{9}$$

$$\begin{aligned} \rho C_p(\bar{u}\bar{T}_{\bar{x}} + \bar{v}\bar{T}_{\bar{y}}) &= k(\bar{T}_{\bar{x}\bar{x}} + \bar{T}_{\bar{y}\bar{y}}) \\ &\quad + \left\{ \mu_\infty + (\mu_o - \mu_\infty) \left(\frac{\sinh^{-1}(\lambda|\bar{\gamma}|)}{\lambda|\bar{\gamma}|} \right)^\sigma \right\} \left\{ 2\bar{v}_{\bar{y}}^2 + (\bar{u}_{\bar{y}} + \bar{v}_{\bar{x}})^2 + 2\bar{u}_{\bar{x}}^2 \right\}. \end{aligned} \tag{10}$$

Now, the Eqs. (8)–(10) are reduced through boundary layer assumptions. Consider the following boundary layer assumptions as

$$\bar{x} = Lx, \bar{y} = \varepsilon Ly, \bar{u} = U_\infty u, \bar{v} = \varepsilon U_\infty v, \bar{p} = \rho U_\infty^2 p, T = \frac{\bar{T} - T_\infty}{T_w - T_\infty}. \tag{11}$$

Equations (8)–(10) after applying Eq. (11) are written as

$$\begin{aligned}
 (uu_x + vu_y) &= -p_x \\
 &+ \text{Re}^{-1} \left[\left\{ \beta + (1 - \beta) \left(\frac{\sinh^{-1} \left(\frac{\text{Re}^{-1}}{\varepsilon} C \sqrt{2\varepsilon^2 v_y^2 + (u_y + \varepsilon^2 v_x)^2 + 2\varepsilon^2 u_x^2} \right)}{\left(\frac{\text{Re}^{-1}}{\varepsilon} C \sqrt{2\varepsilon^2 v_y^2 + (u_y + \varepsilon^2 v_x)^2 + 2\varepsilon^2 u_x^2} \right)} \right)^\sigma \right\} (2u_x) \right]_x \\
 &+ \frac{\text{Re}^{-1}}{\varepsilon^2} \left[\left\{ \beta + (1 - \beta) \left(\frac{\sinh^{-1} \left(\frac{\text{Re}^{-1}}{\varepsilon} C \sqrt{2\varepsilon^2 v_y^2 + (u_y + \varepsilon^2 v_x)^2 + 2\varepsilon^2 u_x^2} \right)}{\left(\frac{\text{Re}^{-1}}{\varepsilon} C \sqrt{2\varepsilon^2 v_y^2 + (u_y + \varepsilon^2 v_x)^2 + 2\varepsilon^2 u_x^2} \right)} \right)^\sigma \right\} (u_y + \varepsilon^2 v_x) \right]_y,
 \end{aligned} \tag{12}$$

$$\begin{aligned}
 \varepsilon^2(uv_x + vw_y) &= -p_y \\
 &+ \text{Re}^{-1} \left[\left\{ \beta + (1 - \beta) \left(\frac{\sinh^{-1} \left(\frac{\text{Re}^{-1}}{\varepsilon} C \sqrt{2\varepsilon^2 v_y^2 + (u_y + \varepsilon^2 v_x)^2 + 2\varepsilon^2 u_x^2} \right)}{\left(\frac{\text{Re}^{-1}}{\varepsilon} C \sqrt{2\varepsilon^2 v_y^2 + (u_y + \varepsilon^2 v_x)^2 + 2\varepsilon^2 u_x^2} \right)} \right)^\sigma \right\} (u_y + \varepsilon^2 v_x) \right]_x \\
 &+ \text{Re}^{-1} \left[\left\{ \beta + (1 - \beta) \left(\frac{\sinh^{-1} \left(\frac{\text{Re}^{-1}}{\varepsilon} C \sqrt{2\varepsilon^2 v_y^2 + (u_y + \varepsilon^2 v_x)^2 + 2\varepsilon^2 u_x^2} \right)}{\left(\frac{\text{Re}^{-1}}{\varepsilon} C \sqrt{2\varepsilon^2 v_y^2 + (u_y + \varepsilon^2 v_x)^2 + 2\varepsilon^2 u_x^2} \right)} \right)^\sigma \right\} (2v_y) \right]_y,
 \end{aligned} \tag{13}$$

$$\begin{aligned}
 (uT_x + vT_y) &= \text{Pr}^{-1} \left(\frac{\text{Re}^{-1}}{\varepsilon^2} \right) (T_{yy} + \varepsilon^2 T_{xx}) \\
 &+ Ec \frac{\text{Re}^{-1}}{\varepsilon^2} \left[\left\{ \beta + (1 - \beta) \left(\frac{\sinh^{-1} \left(\frac{C \text{Re}^{-1}}{\varepsilon} \sqrt{2\varepsilon^2 v_y^2 + (u_y + \varepsilon^2 v_x)^2 + 2\varepsilon^2 u_x^2} \right)}{C \frac{\text{Re}^{-1}}{\varepsilon} \sqrt{2\varepsilon^2 v_y^2 + (u_y + \varepsilon^2 v_x)^2 + 2\varepsilon^2 u_x^2}} \right)^\sigma \right\} \left\{ \begin{aligned} &2\varepsilon^2 v_y^2 + 2\varepsilon^2 u_x^2 \\ &(u_y + \varepsilon^2 v_x)^2 \end{aligned} \right\} \right].
 \end{aligned} \tag{14}$$

Here $Ec = \frac{U_\infty^2}{C_p(T_w - T_\infty)}$, $\text{Pr}^{-1} = \frac{\alpha}{\nu}$, $\text{Re}^{-1} = \frac{\mu_o}{U_\infty \rho L}$ and $C = \sqrt{\frac{\mu_\infty^3 \rho \lambda^2}{\mu_o L}}$.
 For $\text{Re} \gg 1$ and

$$\frac{\text{Re}^{-1}}{\varepsilon^2} \approx O(1) \text{ and } \text{Re}^{-1/2} = O(\varepsilon), \tag{15}$$

the Eqs. (12)–(14) are written without bar are written as

$$u_x + v_y = 0, \tag{16}$$

$$\rho(uu_x + vu_y) = -p_x + \left\{ \mu_\infty + (\mu_o - \mu_\infty) \left(\frac{\sinh^{-1} \left(\lambda \sqrt{u_y^2} \right)}{\lambda \sqrt{u_y^2}} \right)^\sigma u_y \right\}_y, \tag{17}$$

$$p_y = 0, \tag{18}$$

$$\rho C_p (uT_x + vT_y) = kT_{yy} + \left\{ \mu_\infty + (\mu_o - \mu_\infty) \left(\frac{\sinh^{-1} \left(\lambda \sqrt{u_y^2} \right)}{\lambda \sqrt{u_y^2}} \right)^\sigma \right\} u_y^2 \tag{19}$$

along associated boundary conditions

$$\begin{aligned}
 u \left(x, A(x+b)^{\frac{1-m}{2}} \right) &= u_w, \quad v \left(x, A(x+b)^{\frac{1-m}{2}} \right) = 0, \quad T \left(x, A(x+b)^{\frac{1-m}{2}} \right) = T_w \\
 u(x, y \rightarrow \infty) &\rightarrow 0, \quad T(x, y \rightarrow \infty) \rightarrow T_\infty.
 \end{aligned} \tag{20}$$

Now, introduces the similarity transformations to reduce the governing equations into ordinary differential equations as²¹

$$\Psi = \sqrt{v u_w (x+b)} F, \quad \eta = y \sqrt{\frac{u_w}{v(x+b)}}, \quad \theta(\eta) = \frac{T - T_\infty}{(T_w - T_\infty)}. \tag{21}$$

In above Ψ is a stream function and satisfies Eq. (21) by

$$u = \frac{\partial \Psi}{\partial y}, \quad v = -\frac{\partial \Psi}{\partial x}. \tag{22}$$

In view of Eqs. (21) and (22), the main Eqs. (16)–(20) are simplified as

$$mF'^2 - \frac{(m+1)}{2}FF'' = \sigma(1-\beta) \left(\frac{\sinh^{-1}(C_x\sqrt{F'^2})}{C_x\sqrt{F'^2}} \right)^{\sigma-1} \left(-\frac{\sinh^{-1}(C_x\sqrt{F'^2})}{C_x\sqrt{F'^2}} + \frac{1}{\sqrt{1+C_x^2F'^2}} \right) F''' + \left(\beta + (1-\beta) \frac{\sinh^{-1}(C_x\sqrt{F'^2})}{(C_x\sqrt{F'^2})} \right)^\sigma F''', \tag{23}$$

$$-\frac{m+1}{2} \text{Pr} F\theta' = \theta'' + \text{Pr} Ec \left\{ \beta + (1-\beta) \left(\frac{\sinh^{-1}(C_x\sqrt{F'^2})}{C_x\sqrt{F'^2}} \right)^\sigma \right\} F'^2, \tag{24}$$

$$\begin{aligned} f' = 1, f = \alpha, \theta = 1 & \quad \text{at } \eta = B \\ f' \rightarrow 0, \theta \rightarrow 0 & \quad \text{at } \eta = \infty, \end{aligned} \tag{25}$$

where $\beta = \frac{\mu_\infty}{\mu_o}, C_x = \lambda\sqrt{\frac{a^3(x+b)^{3m-1}}{v}}, \alpha = -B\left(\frac{m-1}{1+m}\right)$ and $B = A\sqrt{\frac{a}{v}}$ are constants.

Entropy generation

The rate of entropy generation is defined as

$$\dot{S}_{gen} = \frac{k}{T_\infty^2} (\nabla T)^2 + \frac{\mu}{T_\infty} \bar{\gamma}^2, \tag{26}$$

where

$$(\nabla T)^2 = \bar{T}_x^2 + \bar{T}_y^2. \tag{27}$$

By using Eq. (27) into Eq. (26), we get

$$\dot{S}_{gen} = \frac{k}{T_\infty^2} (\bar{T}_x^2 + \bar{T}_y^2) + \frac{1}{T_\infty} \left\{ \mu_\infty + (\mu_o - \mu_\infty) \left(\frac{\sinh^{-1}(\lambda|\bar{\gamma}|)}{\lambda|\bar{\gamma}|} \right)^\sigma \right\} (2\bar{v}_y^2 + (\bar{u}_y + \bar{v}_x)^2 + 2\bar{u}_x^2). \tag{28}$$

After applying Eq. (11), we get

$$\begin{aligned} \dot{N} = \frac{\text{Re}^{-1}}{\varepsilon^2} (\varepsilon^2 T_x^2 + T_y^2) \\ + \frac{\text{Re}^{-1}}{\varepsilon^2} \text{Pr} EcA \left[\beta + (1-\beta) \left(\frac{\sinh^{-1} \left(\frac{C \text{Re}^{-1} \sqrt{2\varepsilon^2 v_y^2 + (u_y + \varepsilon^2 v_x)^2 + 2\varepsilon^2 u_x^2}}{C \text{Re}^{-1} \sqrt{2\varepsilon^2 v_y^2 + (u_y + \varepsilon^2 v_x)^2 + 2\varepsilon^2 u_x^2}} \right)}{C \text{Re}^{-1} \sqrt{2\varepsilon^2 v_y^2 + (u_y + \varepsilon^2 v_x)^2 + 2\varepsilon^2 u_x^2}} \right)^\sigma \right] \left\{ \begin{aligned} &2\varepsilon^2 v_y^2 + 2\varepsilon^2 u_x^2 \\ &(u_y + \varepsilon^2 v_x)^2 \end{aligned} \right\}, \end{aligned} \tag{29}$$

where $\dot{N} = \frac{T_\infty^2 L^2 v \dot{S}_{gen}}{k(T_w - T_\infty)^2 U_\infty}$ and $A = \frac{T_\infty}{T_w - T_\infty}$.

Equation (28) in view of Eqs. (15) and (29) are written without a bar are written as

$$\dot{S}_{gen} = \frac{k}{T_\infty^2} (T_y^2) + \frac{1}{T_\infty} \left\{ \mu_\infty + (\mu_o - \mu_\infty) \left(\frac{\sinh^{-1}(\lambda\sqrt{u_y^2})}{\lambda\sqrt{u_y^2}} \right)^\sigma \right\} u_y^2. \tag{30}$$

Now, we apply Eq. (21) in Eq. (30) and get the following form

$$\dot{N}_x = \underbrace{\theta''^2}_{\dot{N}_{x,T}} + A \text{Pr} Ec \underbrace{\left\{ \beta + (1-\beta) \left(\frac{\sinh^{-1}(C_x\sqrt{F'^2})}{C_x\sqrt{F'^2}} \right)^\sigma \right\}}_{\dot{N}_{x,v}} F'^2, \tag{31}$$

here $\dot{N}_x = \frac{T_\infty^2 (x+b)^2 v \dot{S}_{gen}}{k(T_w - T_\infty)^2 u_w}$.

The average rate of entropy generation is calculated as

$$\dot{N}_{av} = \int_B^{\infty} \dot{N}_x(\eta) d\eta. \quad (32)$$

Physical parameters

Skin friction coefficient. To measure the shear stress at the wall, a dimensionless parameter known as the skin friction coefficient is utilized. This coefficient is defined as:

$$C_{f\bar{x}} = \frac{\tau_{12} \Big|_{\bar{y}=A(\bar{x}+b)^{\frac{1-m}{2}}}}{\frac{1}{2} \rho u_w^2}. \quad (33)$$

By using the Eqs. (11) and (21), the coefficient is written as

$$C_{f\bar{x}} = 2\text{Re}_x^{-\frac{1}{2}} \left\{ \beta + (1 - \beta) \left(\frac{\sinh^{-1} \left(C\sqrt{F''^2} \right)}{C\sqrt{F''^2}} \right)^\sigma \right\} F'' \Big|_{\eta=B}, \quad (34)$$

here $\text{Re}_x = \frac{u_w(x+b)}{\nu}$ is the local Reynold number.

Nusselt number. The convective heat transfer coefficient in a dimensionless form which is known Nusselt number, is written as

$$Nu_{\bar{x}} = - \frac{k \frac{dT}{d\bar{y}} \Big|_{\bar{y}=A(\bar{x}+b)^{\frac{1-m}{2}}} (\bar{x} + b)}{k(T_w - T_\infty)}. \quad (35)$$

Equation (35) is written after applying Eqs. (11) and (21) as

$$Nu_x = -\text{Re}_x^{\frac{1}{2}} \theta'(B). \quad (36)$$

Solution technique

The numerical result of Eqs. (23) and (24) along Eq. (25) are obtained by using the RK method in the following manner.

Let $F = F_1$, $\theta = G_1$ and find the system of first-order differential equations as

$$F'_1 = F_2, \quad F'_2 = F_3,$$

$$F'_3 = \frac{\frac{(m+1)}{2} F_1 F_3 - m F_2^2}{\left\{ \sigma(1 - \beta) \left(\frac{\sinh^{-1} \left(C_x \sqrt{F_3^2} \right)}{C_x \sqrt{F_3^2}} \right)^{\sigma-1} \left(-\frac{\sinh^{-1} \left(C_x \sqrt{F_3^2} \right)}{C_x \sqrt{F_3^2}} + \frac{1}{\sqrt{1 + C_x^2 F_3^2}} \right) \right\} + \left(\beta + (1 - \beta) \frac{\sinh^{-1} \left(C_x \sqrt{F_3^2} \right)}{\left(C_x \sqrt{F_3^2} \right)} \right)^\sigma}, \quad (37)$$

$$G'_1 = G_2,$$

$$G'_2 = -\text{Pr} Ec \left\{ \beta + (1 - \beta) \left(\frac{\sinh^{-1} \left(C_x \sqrt{F_3^2} \right)}{C_x \sqrt{F_3^2}} \right)^\sigma \right\} F_3^2 - \frac{(m+1) \text{Pr} F_1 G_2}{2}$$

along boundary conditions

$$\begin{aligned} F_2(0) &= 1, \quad F_3(0) = \Omega_1 \\ G_1(0) &= 1, \quad G_2(0) = \Omega_2 \end{aligned} \quad (38)$$

Here Ω_1 and Ω_2 are unknown constants.

Results and discussion

In this portion, the effects of the time scale parameter λ , exponent parameter σ and high shear rate viscosity μ_∞ on the velocity $F'(\eta)$ and temperature $\theta(\eta)$ profiles as well as on skin friction coefficient $C_{f\bar{x}}$ and Nusselt number, Nu_x are examined. The values of dimensionless rheological parameters such as Weissenberg C , Prandtl

number Pr , Eckert Ec , viscosity ratio parameter β , and Reynold number Re are varied during the investigation and calculated in Table 2.

Figure 2a depicts the velocity profile in terms of the time scale parameter. It is evident that the velocity decreases as the parameter increases. It is used to control the behavior of the viscosity curve. Generally, it is noted that viscosity is rapidly decreased from low shear to high shear when the time scale parameter is increased. The parameter is expressed in the form of the Weissenberg number, indicating a decline in the velocity. Furthermore, the profile's behavior remains almost constant at all values of the x , but the velocity boundary layer thickness

x ↓ C	λ			μ_∞		
	$\mu_\infty = 0.03$			$\lambda = 0.7$		
	0.5	0.7	0.9	0.01	0.02	0.03
2	2.05	2.87	3.68	2.87	2.87	2.87
3	7.87	11.02	14.16	11.02	11.02	11.02
4	21.50	30.11	38.71	30.11	30.11	30.11
$10^{-6} \times Ec$						
2	0.02	0.02	0.02	0.02	0.02	0.02
3	1.53	1.53	1.53	1.53	1.53	1.53
4	6.92	6.92	6.92	6.92	6.92	6.92
Re						
2	4297	4297	4297	4297	4297	4297
3	16,507	16,507	16,507	16,507	16,507	16,507
4	45,107	45,107	45,107	45,107	45,107	45,107
Pr						
-	10	10	10	10	10	10
β	0.3	0.3	0.3	0.1	0.2	0.3

Table 2. The value of different dimensionless parameters when $\rho = 1100, C_p = 4000, \mu_o = 0.1, m = 3, \sigma = 1, a = 0.01, A = 0.02, b = 0.5, T_w - T_\infty = 30$ and $k = 40$.

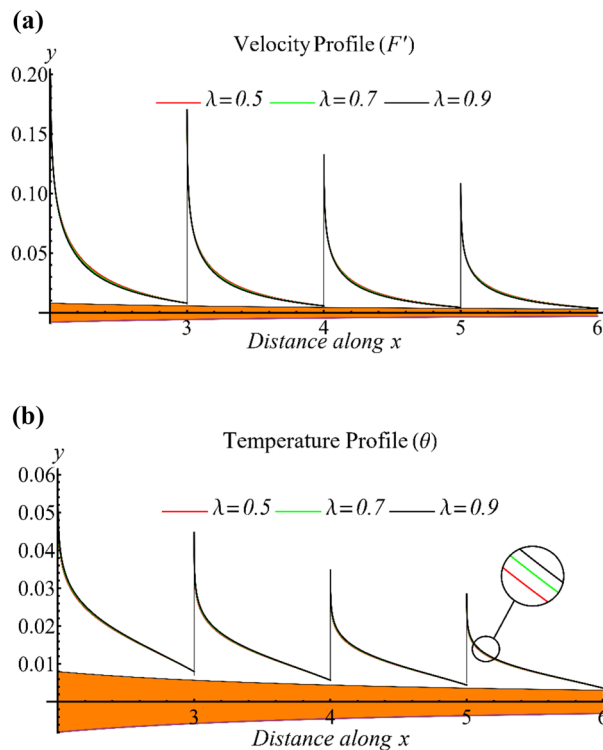


Figure 2. (a) The influence of the time sale parameter on the velocity profile. (b) The influence of the time sale parameter on the temperature profile.

decreases as the distance from the origin in the parallel direction increases. Figure 2b shows the temperature profile for different time scale parameter values. As the parameter increases, the temperature also rises. Additionally, the temperature distribution remains constant for every value of the x , but the thermal boundary layer thickness decreases more than the velocity boundary layer thickness.

Figure 3a presents the influence of the exponent parameter on the velocity profile. It is observed that the velocity decreases as the parameter increases, which is attributed to the increase in viscosity with respect to the shear rate under the given flow conditions. Figure 3b depicts the impact of the parameter on the temperature profile, which displays an increase in the temperature profile with an increasing parameter value. Notably, both profiles exhibit a similar trend at different values of x , as shown in Figs. 2 and 3.

Figure 4a reveals the effect of high shear rate viscosity on the velocity profile, which demonstrates an increase in the velocity profile with increasing high shear rate viscosity. This viscosity appears in the viscosity ratio parameter and implies a reduction in velocity as the parameter value increases. Furthermore, Fig. 4b displays the temperature profile under the influence of high shear rate viscosity, indicating a decrease in temperature as the viscosity ratio parameter increases.

Figure 5 illustrates the impact of different parameters on the average rate of entropy generation. It is observed that entropy generation increases when the time scale parameter is increased, owing to the dominant influence of viscous irreversibility compared to thermal irreversibility. A similar trend of entropy generation is observed in the case of the exponent parameter, where thermal irreversibility decreases, but viscous irreversibility increases significantly, resulting in an enhancement of entropy generation. When the difference between low and high shear rate viscosities is reduced by increasing the high shear rate viscosity, entropy generation decreases due to the decrease in viscous irreversibility.

The numerical values of the skin friction coefficient under the influence of the time scale parameter, exponent parameter, and high shear rate viscosity at different values of the parameter are presented in Table 3. The coefficient magnitude decreases with increasing time scale and exponent parameters but increases with an increase in high shear rate viscosity. The negative sign of the coefficient indicates that the sheet exerts a shear stress on the fluid. The results of the Nusselt number in relation to the aforementioned parameters are presented in Table 4. An increase in the time scale and exponent parameters results in a decrease in the Nusselt number, while high shear rate viscosity leads to an increase in the Nusselt number.

Conclusions

The present investigation examines the heat and mass flow behaviors of a shear-thinning fluid through a generalized Powell–Eyring model. This study introduces a higher shear rate viscosity, time scale and exponent parameters in the flow modeling, which has not been previously done with the Powell–Eyring model. The effects of these parameters on the velocity and temperature profiles are summarized as follows:

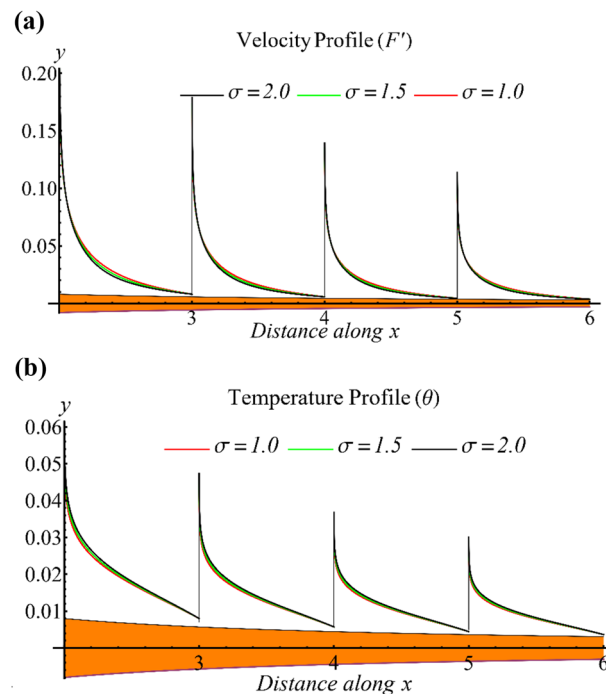


Figure 3. (a) The influence of the exponent parameter on the velocity profile. (b) The influence of the exponent parameter on the temperature profile.

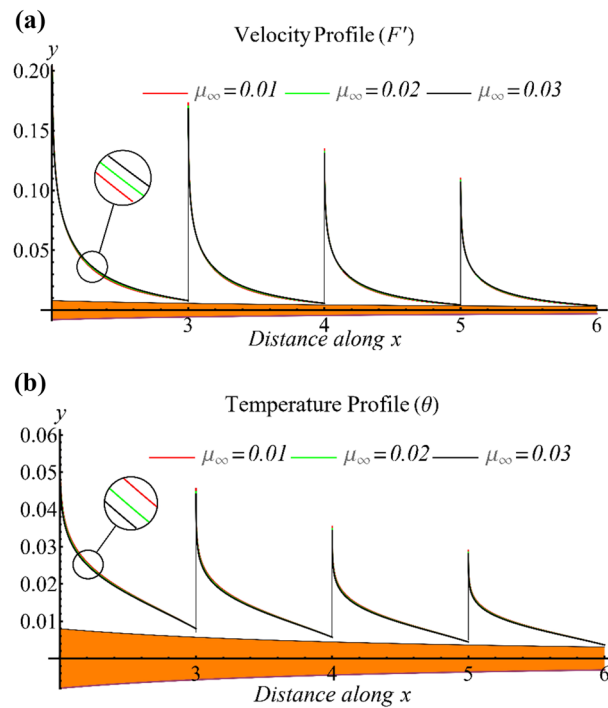


Figure 4. (a) The influence of high shear rate viscosity on the velocity profile. (b) The influence of high shear rate viscosity on the temperature profile.

- Upon increasing the time scale parameter, a consequential reduction in viscosity occurs, leading to a decrease in the velocity profile and an increase in the temperature profile. The corresponding increase in the time scale parameter leads to an increase in the average entropy generation.
- An increase in the exponent parameter accentuates the shear thinning effects, resulting in a decrease in the velocity profile and an increase in the temperature profile. This parameter also causes an increase in the average entropy generation.
- Regarding the numerical values, an increase in the time scale and exponent parameters leads to a decrease in the skin friction coefficient. However, an increase in shear rate viscosity causes the skin friction coefficient to increase. Conversely, the Nusselt number demonstrates an opposing trend in comparison to the skin friction coefficient concerning these parameters.

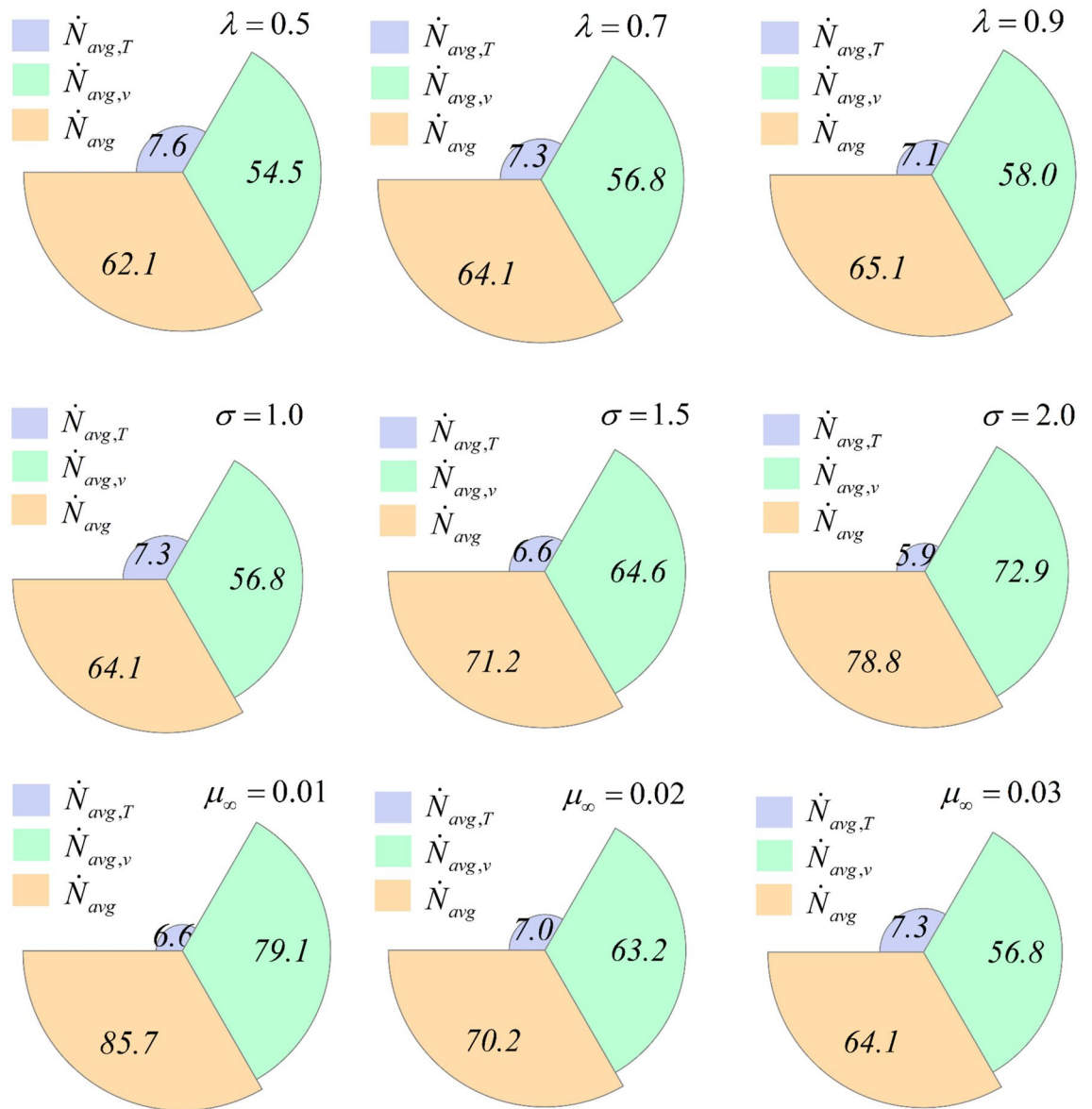


Figure 5. The average rate of entropy generation under different parameter effects.

	λ			σ			μ_∞		
x	0.5	0.7	0.9	0.010	0.015	0.020	0.01	0.02	0.03
2	0.04005	0.03623	0.03364	0.03786	0.03204	0.02572	0.03390	0.03897	0.04404
3	0.01399	0.01296	0.01233	0.01362	0.00993	0.00699	0.00921	0.01270	0.01618
4	0.00695	0.00663	0.00644	0.00701	0.00481	0.00323	0.00388	0.00618	0.00847

Table 3. The values of local Skin friction number $-C_{fx}$ under the influence of different parameters.

	λ			σ			μ_∞		
x	1.0	1.5	2.0	0.010	0.015	0.020	0.01	0.02	0.03
2	125.143	385.727	370.563	123.398	119.052	114.371	118.945	121.491	123.398
3	245.281	241.860	239.285	241.860	233.341	224.168	233.133	238.123	241.860
4	405.464	399.810	395.553	399.810	385.727	370.563	385.383	393.632	399.810

Table 4. The values of local Nusselt number $-Nu_x$ under the influence of different parameters.

Data availability

The datasets used and/or analyzed during the current study are available from the corresponding author upon request.

Received: 21 January 2023; Accepted: 21 May 2023

Published online: 24 May 2023

References

- Shafiq, A., Mebarek-Oudina, F., Sindhu, T. N. & Abidi, A. A study of dual stratification on stagnation point Walters' B nanofluid flow via radiative Riga plate: A statistical approach. *Eur. Phys. J. Plus* **136**, 1–24 (2021).
- Shafiq, A., Rasool, G., Khaliq, C. M. & Aslam, S. Second grade bioconvective nanofluid flow with buoyancy effect and chemical reaction. *Symmetry* **12**(4), 621 (2020).
- Ostwald, W. Ueber die rechnerische Darstellung des Strukturgebietes der Viskosität. *Kolloid Z.* **47**, 176–187 (1929).
- Cross, M. M. Rheology of non-Newtonian fluids: A new flow equation for pseudoplastic systems. *J. Colloid Sci.* **20**, 417–437 (1965).
- Carreau, P. J. Rheological equations from molecular network theories. *Trans. Soc. Rheol.* **16**, 99–127 (1972).
- Yoon, H. K. & Ghajar, A. J. A note on the Powell–Eyring fluid model. *Int. Commun. Heat Mass Transf.* **14**(4), 381–390 (1987).
- Schetz, J. A. & Fuhs, A. E. (eds) *Handbook of Fluid Dynamics and Fluid Machinery* (Wiley, 1996).
- Riaz, A., Ellahi, R. & Sait, S. M. Role of hybrid nanoparticles in thermal performance of peristaltic flow of Eyring–Powell fluid model. *J. Therm. Anal. Calorim.* **143**(2), 1021–1035 (2021).
- Nazeer, M. Numerical and perturbation solutions of cross flow of an Eyring–Powell fluid. *SN Appl. Sci.* **3**(2), 1–1 (2021).
- Oke, A. S. Theoretical analysis of modified Eyring–Powell fluid flow. *J. Taiwan Inst. Chem. Eng.* **8**, 104152 (2021).
- Rahimi, J., Ganji, D. D., Khaki, M. & Hosseinzadeh, K. Solution of the boundary layer flow of an Eyring–Powell non-Newtonian fluid over a linear stretching sheet by collocation method. *Alex. Eng. J.* **56**(4), 621–627 (2017).
- Verma, A. K., Gautam, A. K., Bhattacharyya, K., Banerjee, A. & Chamkha, A. J. Boundary layer flow of non-Newtonian Eyring–Powell nanofluid over a moving flat plate in Darcy porous medium with a parallel free-stream: Multiple solutions and stability analysis. *Pramana* **95**(4), 1–8 (2021).
- Akgül, A. Reproducing kernel Hilbert space method based on reproducing kernel functions for investigating boundary layer flow of a Powell–Eyring non-Newtonian fluid. *J. Taibah Univ. Sci.* **13**(1), 858–863 (2019).
- Imran, M., Abbas, Z. & Naveed, M. Flow of Eyring–Powell liquid due to oscillatory stretchable curved sheet with modified Fourier and Fick's model. *Appl. Math. Mech.* **42**(10), 1461–1478 (2021).
- Ibrahim, W. & Hindebu, B. Magnetohydrodynamic (MHD) boundary layer flow of Eyring–Powell nanofluid past stretching cylinder with Cattaneo–Christov heat flux model. *Nonlinear Eng.* **8**(1), 303–317 (2019).
- Kumar, D., Ramesh, K. & Chandok, S. Mathematical modeling and simulation for the flow of magneto-Powell–Eyring fluid in an annulus with concentric rotating cylinders. *Chin. J. Phys.* **1**(65), 187–197 (2020).
- Gholinia, M., Hosseinzadeh, K., Mehrzadi, H., Ganji, D. D. & Ranjbar, A. A. Investigation of MHD Eyring–Powell fluid flow over a rotating disk under effect of homogeneous–heterogeneous reactions. *Case Stud. Therm. Eng.* **1**(13), 100356 (2019).
- Salawu, S. O., Kareem, R. A. & Shonola, S. A. Radiative thermal criticality and entropy generation of hydromagnetic reactive Powell–Eyring fluid in saturated porous media with variable conductivity. *Energy Rep.* **1**(5), 480–488 (2019).
- Madhu, M., Shashikumar, N. S., Gireesha, B. J. & Kishan, N. Thermal analysis of MHD Powell–Eyring fluid flow through a vertical microchannel. *Int. J. Ambient Energy* **8**, 1–9 (2021).
- Çolak, A. B., Shafiq, A. & Sindhu, T. N. Modeling of Darcy–Forchheimer bioconvective Powell Eyring nanofluid with artificial neural network. *Chin. J. Phys.* **1**(77), 2435–2453 (2022).
- Fang, T., Zhang, J. & Zhong, Y. Boundary layer flow over a stretching sheet with variable thickness. *Appl. Math. Comput.* **218**(13), 7241–7252 (2012).

Acknowledgments

The authors extend their appreciation to the Deanship of Scientific Research at King Khalid University, Abha, Saudi Arabia for funding this work through Large Groups Project under grant number RGP2/51/44.

Author contributions

M.H., and M.A. drafted and completed the original draft. Usman has done writing, reviewing, and editing. T.M. and M.A. have prepared a paper according to the reviewer's comments.

Competing interests

The authors declare no competing interests.

Additional information

Correspondence and requests for materials should be addressed to U.

Reprints and permissions information is available at www.nature.com/reprints.

Publisher's note Springer Nature remains neutral with regard to jurisdictional claims in published maps and institutional affiliations.



Open Access This article is licensed under a Creative Commons Attribution 4.0 International License, which permits use, sharing, adaptation, distribution and reproduction in any medium or format, as long as you give appropriate credit to the original author(s) and the source, provide a link to the Creative Commons licence, and indicate if changes were made. The images or other third party material in this article are included in the article's Creative Commons licence, unless indicated otherwise in a credit line to the material. If material is not included in the article's Creative Commons licence and your intended use is not permitted by statutory regulation or exceeds the permitted use, you will need to obtain permission directly from the copyright holder. To view a copy of this licence, visit <http://creativecommons.org/licenses/by/4.0/>.

© The Author(s) 2023